Vol. 29 (1998) *ACTA PHYSICA POLONICA B* No 6

ON MICROSCOPIC SIMULATIONS OF SYSTEMS WITH MODEL CHEMICAL REACTIONS* **

Jerzy Gorecki

Institute of Physical Chemistry, Polish Academy of Sciences
Kasprzaka 44/52, 01-224 Warsaw, Poland
College of Science
Al.Lotnikow 32/46, 02-668 Warsaw, Poland
Interdisciplinary Ccenter for Mathematical and Computational Modelling
Pawińskiego 5A, 02-106 Warsaw, Poland

and Joanna N. Gorecka

Institute of Physics, Polish Academy of Sciences
Al. Lotnikow 32/46, 02-668 Warsaw, Poland

(Received February 19, 1998)

Large scale computer simulations of model chemical systems play the role of idealized experiments in which theories may be tested. In this paper we present two applications of microscopic simulations based on the reactive hard sphere model. We investigate the influence of internal fluctuations on an oscillating chemical system and observe how they modify the phase portrait of it. Another application, we consider, is concerned with the propagation of a chemical wave front associated with a thermally activated reaction. It is shown that the nonequilibrium effects increase the front velocity if compared with the velocity of the front generated by an nonactivated process characterized by the same rate constant.

PACS numbers: 82.20. Mj, 82.20. Wt, 82.40. Bj

1. Introduction

Nonlinear phenomena observed in far-from-equilibrium chemical systems have attracted a lot of scientific attention in the recent years [1–7]. The theoretical description of these phenomena requires the methods, which go

---

[*] Presented at the Marian Smoluchowski Symposium on Statistical Physics, Zakopane, Poland, September 1–10, 1997.

[**] This work was supported by the grants KBN 3T09A 120 08 and KBN 2 T03 B018 10 provided by the Polish State Committee for Scientific Research.

beyond the classical chemical kinetics based on the mass action law. In the case of very fast chemical reactions, for which the relaxation processes are slow if compared with the reaction rates, one may expect that the distribution of the energetic states of reagents is different from the equilibrium one and thus the rate constants differ from their equilibrium values. On the other hand, in nonlinear chemical systems fluctuations play an important role because for example they may switch the system from one basin of attraction to another. In order to take fluctuations into account one has to use the probabilistic description instead of the classical phenomenology. It is difficult to test new theoretical ideas by comparing their results with experiments because not so many of them were performed for sufficiently simple chemical system to be treated by a theory. In this respect large scale microscopic simulations of model chemical systems play an important role because they allow one to compare theory with idealized experiments for which all the elementary processes are known.

Although the number of particles involved in simulations is very small if compared with real systems, nerveless the simulations which involve millions of particles are usually sufficient to give us information on nonequilibrium behavior. The most popular simulation techniques used for large scale simulations of model chemical systems are the lattice gas automata [8] and the direct simulations of Boltzmann equation [9]. These methods are very efficient from numerical point of view and can be easily applied for simulations involving millions of particles, but on the other hand they involve serious simplifications. In the both cases the reactants are represented as structureless particles and the parameter describing the chemical properties of a particle does not have any influence on the interaction with the other particles of the system. The high efficiency of computer algorithms based on the lattice gas model is achieved by introducing significant restrictions on system's geometry. Both space and time are described by discrete variables. Particles may occupy the lattice nodes only and may jump to the neighboring nodes within a single time step. Therefore the speed of the particles remains the same and, for example, the simulations of thermally activated processes are not possible. The Bird method (direct simulation of Boltzmann equation) [9] is also frequently used for large scale simulations. According to the method the system is divided into cells and the free flow of particles between cells is allowed. However, in order to speed simulations up, only the interactions between particles belonging to the same cell are taken into account. Moreover the interacting (reacting) particles are randomly selected without considering their positions in space. In the consequence the short scale spatial correlations are completely neglected in this approach, which makes it appropriate for low density systems only.

In this paper we are concerned with simulations based on the molecular dynamics (MD) for reactive hard spheres [10]. This method requires more involved computations than the techniques mentioned above, but it also allows one to study systems composed of many millions particles for times of the order of 10^{-9}s. It does not introduce restrictions on the energies of molecules, thus it can be easily adopted for simulations of thermally activated process. In the simplest version of the method all particles are described as hard spheres and short scale correlations related to the excluded volume effect appear in a natural way. Such molecular dynamics simulations for reactive hard spheres may be easily performed for different systems's densities, even very high.

Here we present two applications of the MD method. First we investigate the influence of internal fluctuations on a chemical system, which according to the phenomenological kinetic equations exhibit oscillations in concentrations of reactants. The simulations indicate that the character of evolution observed in MD simulations depends on how strong is the attraction towards a limit cycle. Another problem considered is related with nonequilibrium effects in a system with a thermally activated, autocatalytic reaction $A + B \rightarrow A + A$ and the influence of them on the wave front propagation. We show that a simple phenomenology which takes into account coupled kinetic equations for concentration and density of energy gives quite accurate description of influence of the nonequilibrium effects on wave front velocity.

2. The simulation technique

There is no doubt that molecular dynamics [11] is the most appropriate technique for microscopic simulations. However this method is the most demanding from computational point of view and in the case of large scale systems supercomputing facilities are necessary. Here we present a simplified version of the technique, which allows one to perform large scale simulations of the system with thermoneutral chemical processes. The method is originates from the molecular dynamics for reacting hard spheres [10]. According to it the molecules are represented by structureless hard spheres and the chemical identity parameter does not have any influence on the mechanical motion of a sphere. A chemical reaction may occur when spheres representing their reactants collide. As the time of collision between hard spheres is equal to zero there is a clear separation of time scales related to the reaction and to the motion of particles.

In the case of thermoneutral reactions all the reactive collisions are elastic from the mechanical point of view. The trajectory which describes the motion of molecules is an equilibrium trajectory for a system of spheres.

Therefore one can easily simulate systems with different thermoneutral processes using a prerecorded trajectory as the database on the consecutive collisions and just checking if they lead to reactions or not. A significant increase in the scale of simulations can be achieved if the periodic expansion of the system is used [12]. The periodic boundary conditions mean that the simulated system is regarded as an elementary cell in an infinite system, which is invariant with respect to the translations by the vectors of the side length. Knowing the evolution within a single cell one has the information about positions and velocities for corresponding (by symmetry) particles in all its replicas. Therefore, using a prerecorded data with the sequence of elastic collisions one can obtain the evolution of a system which is extended by a number of cells in each direction. Of course, the periodic boundary conditions remain satisfied for the extended system too.

Let us stress that if a chemical identity of molecules is neglected than such expansion does not bring us any new information , as the evolution in all cells of the extended system is identical. Moreover, it may lead to wrong conclusions as the correlations extending over a single cell are duplicated by the artificially introduced periodicity. However, for a multicomponent chemical system, in which the translational motion is not related to chemical identity, the situation is different. First, different chemical compositions may be initialized in various cells by marking the equivalent (by periodicity) spheres in a different way. Next, a steric factor if it is not equal to unity, differentiates the "chemical" evolution, because a collision between the same objects may be reactive in one cell and nonreactive in another one. Thanks to the periodic boundary conditions a free flow of molecules, between the neighboring cells is ensured. Therefore, one can obtain the evolution of a system which is much larger than the original one.

3. Studies on fluctuations around a limit cycle

The chemical model of a system exhibiting oscillation consists of the following elementary (bimolecular) reactions [13]:

$$R + S \underset{k_{-1}}{\overset{k_1}{\rightleftharpoons}} V + S\,, \tag{1}$$

$$V + E \underset{k_{-2}}{\overset{k_2}{\rightleftharpoons}} X + S\,, \tag{2}$$

$$X + S \rightarrow^{k_3} E + U\,, \tag{3}$$

$$X + V \underset{k_{-4}}{\overset{k_4}{\rightleftharpoons}} Y + S\,, \tag{4}$$

$$V + S \underset{k_{-5}}{\overset{k_5}{\rightleftharpoons}} U + S\,. \tag{5}$$

This scheme is a modification of the model of an open chemical system with a catalytic (enzymatic) reaction, inhibited by an excess of its reactant V. The reactant V is transformed to the product U with E as the catalyst (steps (2) and (3)). This part of the scheme is the well known Langmuir–Hinshelwood mechanism of catalytic reactions (or the Michaelis–Menten kinetics for enzymatic reactions). Step (4) is the inhibition of the Langmuir–Hinshelwood mechanism by an excess of the reactant V. Moreover, the reactant V is transformed directly to the product U in the step (5). It is assumed, that S is a solvent, whose concentration is maintained constant. The system is open, due to step (1), in which the reactant V is produced from the reagent R, whose concentration is also maintained constant.

Let us consider a homogeneous system in which reactions (1-5) proceed. According to the mass action law, its evolution is described by five kinetic equations for V, U, E, X and Y, but it is easy to notice that $E(t)+X(t)+Y(t)=E_0$ is constant and it is the first integral of the system. Therefore, the phenomenological description is based on kinetic equations for four variables, which have the form:

$$\begin{aligned}\frac{dV}{dt} &= k_1RS - k_{-1}VS - k_2VE + k_{-2}XS \\ &\quad -k_4VX + k_{-4}(E_0 - E - X)S - k_5VS + k_{-5}US\,, \qquad (6)\\ \frac{dE}{dt} &= -k_2VE + (k_{-2}+k_3)XS\,, \qquad (7)\\ \frac{dX}{dt} &= k_2VE - (k_{-2}+k_3)XS - k_4VX + k_{-4}(E_0 - E - X)S\,, \qquad (8)\\ \frac{dU}{dt} &= k_3XS + k_5VS - k_{-5}US\,, \qquad (9)\end{aligned}$$

where, for convenience, the symbols of the reagents are used to denote their concentrations.

Usually the description of an catalytic system can be simplified provided that the concentration of the catalyst is much smaller than the concentrations of other reactants. However the MD simulations are the most efficient if the concentrations of all reagents do not differ significantly and we have to use the whole set of kinetic equations.

For an appropriate choice of the rate constants and the concentrations of S, R and E_0 the system of equations (6)–(9) exhibit the Hopf bifurcation and can have a stable limit cycle as the asymptotic trajectory. It may be checked that the shape and the stability of the limit cycle strongly depend on the value of k_2. Fixing the values of the other parameters as equal to: $S = 0.1$, $R = 0.5$, $E_0 = 0.2$ and $k_1 = 0.1$, $k_{-1} = 0.12$, $k_{-2} = 0.1$, $k_3 = 3.9$, $k_4 = 1.0$, $k_{-4} = 4.0$, $k_5 = 0.1$, $k_{-5} = 0.1$ we find that the Hopf bifurcation occurs at $k_2 \cong 5.914$. In simulations we considered two values of k_2: $k_2 = 6.0$ and $k_2 = 8.0$. At $k_2 = 6.0$ the system is close to the bifurcation and should be much more sensitive to internal fluctuations than for $k_2 = 8.0$. For $k_2 = 8.0$ we have a large, strongly attractive limit cycle (drawn in Fig. 1(a) using a solid line). The cycle obtained $k_2 = 6.0$ is much smaller and less attractive (see Fig. 1(b)). Nevertheless, the periods of both limit cycles are almost equal ($T_{\mathrm{ph}} = 640$ for $k_2 = 6.0$ and $T_{\mathrm{ph}} = 653$ for $k_2 = 8.0$).

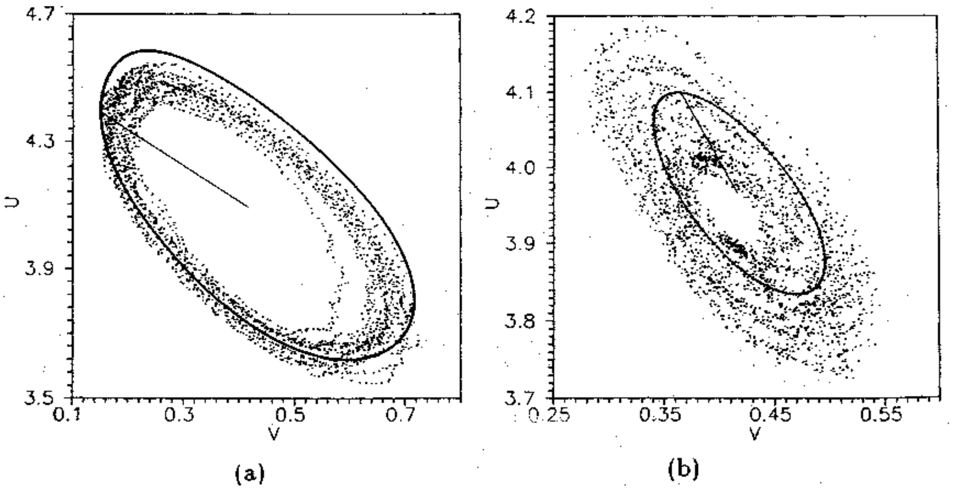

Fig. 1. The comparison of the phenomenological limit cycle (the thin solid line) with the results of MD simulations (points). The interval links C_{MD} with a point for which $\phi = 0$. (a) — $\Omega = 10800$, $k_2 = 8$; (b) — $\Omega = 10800$, $k_2 = 6$.

A system with reactions (1)–(5) can be easily modelled using MD technique for reactive hard spheres because all processes are bimolecular. If we assume that all reactions (1)–(5) are thermoneutral then periodically extended MD technique for reactive hard spheres [12] can be easily applied to simulate the time evolution of the system. For simplicity all reactants (E, R, S, U, V, X and Y) are represented by hard spheres with the same mass (m) and diameter (d). In order to control the rates of chemical processes the steric factors are introduced (they are denoted as $s_i, s_{-i}, i = 1, 5$). If a collision between spheres representing reagents of one of the process (1)–(5) occurs, then a random number generator is called by the program and if the obtained random number is smaller that the corresponding steric factor then the collision is regarded as a reactive one. After such collision the chemical identity parameters of the spheres involved are modified according to the reaction scheme (1)–(5). Otherwise the collision is nonreactive one and the spheres retain their chemical identities.

In order to keep the concentrations of the reactants R and S constant we use the procedure described in Ref. [14]. Nonreactive particles which play the role of reservoir of R and S molecules are present in the simulated system. If a particle of S (R) vanishes in one of the reactions then simultaneously a randomly selected particle of reservoir is transformed into S (R), respectively. On the other hand if a particle of S (R) appears then a randomly chosen particle of S (R) becomes a particle of reservoir. These processes have no influence on the dynamics of the system because they do not participate in (1)–(5). The random transformations between the reservoir particles and reactants introduce a stirring in the simulated system which helps to destroy the nonequilibrium spatial correlations between molecules of reactants [15].

The results presented below have been obtained by a periodic expansion of the system of $N = 400$ hard spheres placed in a cubic box with the side length $l = 12.5 * d$ (and thus the packing fraction is $\eta \approx 0.11$). The prerecorded trajectory contained information on $20,160,000$ collisions (over $50,000$ collision per one sphere). It is assumed that the density of the system is 8 [mol/l], which corresponds to the volume of the original box equal to $83.(3) * 10^{-21}\mathrm{cm}^3$. If the volume is rescaled to units $10^3\mathrm{cm}^3/N = 1.6(6) * 10^{-21}\mathrm{cm}^3$ (N is the Avogadro number) then the volume of the original box is equal to 50 in these units. In the new units the number concentrations of reagents are numerically equal to the concentrations in [mol/l] in the phenomenological equations. The simulations were performed for the system expanded by 6 box lengths in all directions, which gives the volume Ω equal to 10800.

The initial concentrations of reagents represent a point on the phenomenological limit cycle. At the beginning the chemical identities are assigned to spheres in a random way and all remaining spheres are marked as the reservoir particles. The values of steric factors for MD simulations were obtained by scaling the phenomenological rate constants by 0.06(6), which leads to: $s_1 = 0.006(6), s_{-1} = 0.008, s_{-2} = 0.006(6), s_3 = 0.26, s_4 = 0.066(6), s_{-4} = 0.266(6), s_5 = 0.006(6), s_{-5} = 0.006(6)$ for reactions (1)–(5) respectively. For $k_2 = 8$ we have $s_2 = 0.533(3)$, whereas for $k_2 = 6$ the steric factor $s_2 = 0.4$. In order to adjust the frequencies of reactive collisions to the rate constants k_i appearing in the kinetic equations the real time of the MD simulations t_{MD} is rescaled to the phenomenological time t according to:

$$t = \frac{1}{8} d^2 g \sqrt{\frac{\pi k_{\mathrm{B}} T}{m}} \frac{s_1}{k_1} t_{\mathrm{MD}} \,, \tag{10}$$

where $g = 1.35$ is the value of the radial distribution function at the sphere diameter d for the system of spheres characterized by the assumed density, k_{B} is the Boltzmann constant and T is the temperature of our system ($T = 300$). The results shown in Figures 2 and 4 are presented in phenomenological time scale. The prerecorded trajectory allowed us to study processes, which in phenomenological time scale last over $t_e \cong 840$ which means that they are only slightly longer than one period. In order to study the long time behavior of the system we started new simulation program from concentrations obtained at the end of the previous one. This procedure corresponds to the instant homogenization of the system after each t_e interval and it destroys possible spatial correlations, which may appear between particles representing different reactants.

The time evolution of concentrations of U obtained in MD simulations for $k_2 = 8$ and $k_2 = 6$ are shown in Figures 2(a), 2(b), respectively. Stars mark the intervals t_e which correspond to individual simulation programs. Both concentrations exhibit quite regular oscillations and fluctuations can be seen mainly around the extrema. Despite of fluctuations the periods of MD oscillations (the average time between consecutive maxima of U) are in a good agreement with phenomenology and equal to $t_{\mathrm{MD}} = 657$ for $k_2 = 8$ and $t_{\mathrm{MD}} = 667$ for $k_2 = 6$. As expected in the case of $k_2 = 6$ the limit cycle is much less attractive as compared with $k_2 = 8$ and the fluctuations of the amplitude of oscillations are much more pronounced than in the previous case.

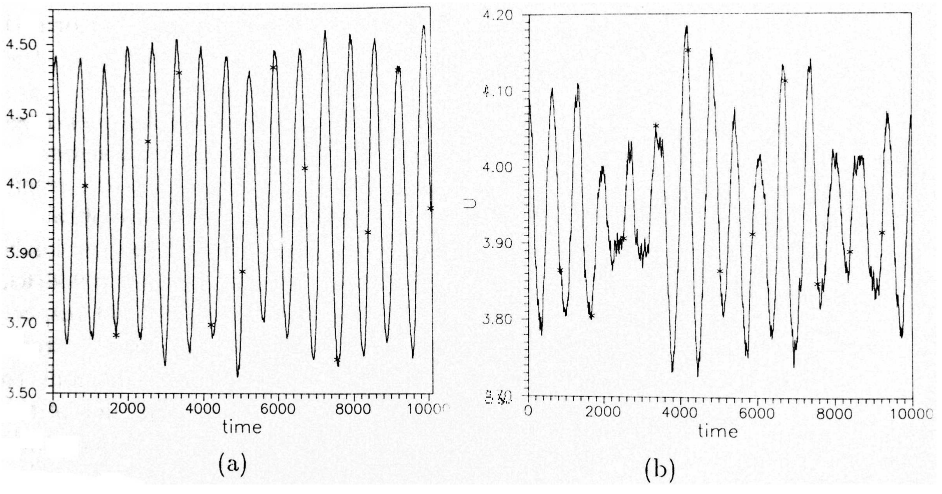

(a) (b)

Fig. 2. The concentration of U as a function of time. Stars mark the ends of intervals t_e which correspond to the length of individual simulation programs. (a)—$\Omega = 10800$, $k_2 = 8$; (b)—$\Omega = 10800$, $k_2 = 6$.

Qualitative differences in evolutions of systems with $k_2 = 6$ and $k_2 = 8$ can be clearly observed on the projection of trajectories from 4-dimensional phase space onto the $V \times U$ plane. The phenomenological limit cycle (the solid line) is compared with the results of simulations (points). For $k_2 = 8$ (Fig. 1(a)) points form a cycle and their distribution becomes narrower when the size of the system increases. The right part of the cycle obtained in MD simulations is shifted towards smaller values of U as compared with phenomenology which we believe is related to influence of the nonequilibrium effects on spatial correlations between concentrations of reactants [15]. For $k_2 = 6$ the behavior is shown in Fig. 1(b). The MD trajectory is widely scattered in the neighborhood of the phenomenological limit cycle but the volcano crater like structure is still clearly visible. Here the influence of nonequilibrium effects is hidden by very large fluctuations.

In order to give quantitative description of the differences between simulations and phenomenology let us consider the projection of the limit cycle on $V \times U$ plane. Let us define the center of the limit cycle $C = (V_c, U_c)$ as the point on $V \times U$ plane the coordinates of which are the values of concentrations averaged over the cycle. The phenomenology gives the following coordinates of C: for $k_2 = 6$ we have $V_c = 0.416565$ and $U_c = 3.96475$ whereas for $k_2 = 8$: $V_c = 0.416609$ and $U_c = 4.08982$. By averaging MD results we have obtained C_{MD} which coordinates are: $V_c = 0.414, U_c = 3.933$ for $k_2 = 6$ and $V_c = 0.413, U_c = 4.048$ for $k_2 = 8$. It is noteworthy that the MD results are in a good agreement with the phenomenological position of the center and that the difference in coordinates of C for $k_2 = 6$ and $k_2 = 8$ predicted by phenomenology is confirmed by the MD simulations.

Knowing the center one can introduce parameterization of the projected limit cycle using radius and phase. The radius is defined as the length of vector from the center towards a given point on the cycle. To define the phase ϕ one needs to specify the direction which corresponds to $\phi = 0$. In our analysis it is the direction from the center C towards the point P representing the initial values of V and U. The projection of the vector $\vec{CP}$ onto $V \times U$ is marked in Fig. 1. The phase corresponding to any other point Q on the phenomenological limit cycle can be calculated as the angle between vectors $\vec{CP}$ and $\vec{CQ}$. In this way we define the phenomenological radius as a function of the phase ϕ.

Similar procedure may be applied for the analysis of results obtained in MD simulations, but in this case C_{MD} is used instead if C. The radius and the phase characterizing a point O representing a state of simulated system are defined as the length of $C_{\vec{\mathrm{MD}}}O$ and the angle between $C_{\vec{\mathrm{MD}}}P$ and $C_{\vec{\mathrm{MD}}}O$ respectively. The phase is positive for the clockwise direction because in this direction the system rotates. The comparison of $\phi(t)$ (in 2π units) coming from both phenomenology and MD is presented in Fig. 3

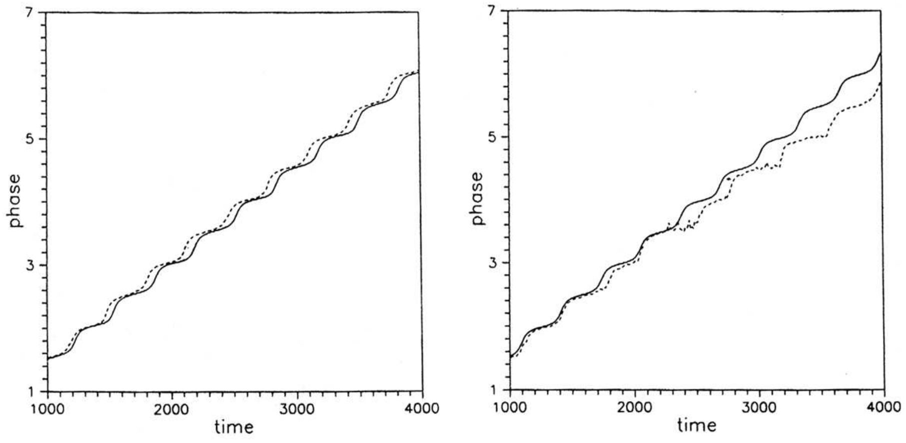

(a) (b)

Fig. 3. The phase ϕ as a function of time. The solid line shows the solution of phenomenological kinetic equations, the dashed line is obtained in MD simulations. (a)—$\Omega = 10800$, $k_2 = 8$; (b)—$\Omega = 10800$, $k_2 = 6$.

where the solid line shows the phenomenological results and the dashed line comes from the simulations. The considered range of times was selected in order to see what is the influence of pronounced fluctuations in $U(t)$ (*cf.* Fig. 2(b)) on the phase. It is seen that within a single period the phase as a function of time has two regions of slow increase which correspond to the extrema of $U(t)$ and two regions of rapid increase related to the intervals in which the changes in $U(t)$ are large. For $k_2 = 8$ we get good agreement between the phenomenology and simulations. Small shifts in MD phase with respect to the phenomenological one are visible in regions the phase changes slowly. In the case of $k_2 = 6$ the regions in which the system's evolutions looks stochastic give plateau's in which MD phase is nearly constant. The influence of fluctuations can be seen more clearly if we consider the angular velocity. In MD simulations we record approximately 7000 points of trajectory $(v(t), u(t))$ per a single period. They are grouped into sets consisting 100 points. The angular velocity ($\omega = \frac{d\phi}{dt}$) and its dispersion are separately calculated for each group. The angular velocity as the function of phase $\omega(\phi)$ is shown in Fig. 4. The function has two maxima per period and the values of ω change by an order of magnitude. For $k_2 = 8$ we have a good agreement between the phenomenological $\omega(\phi)$ and the results of simulations. In the case of $k_2 = 6$ the differences are much larger and the areas in which dispersion of ω is large correspond to regions

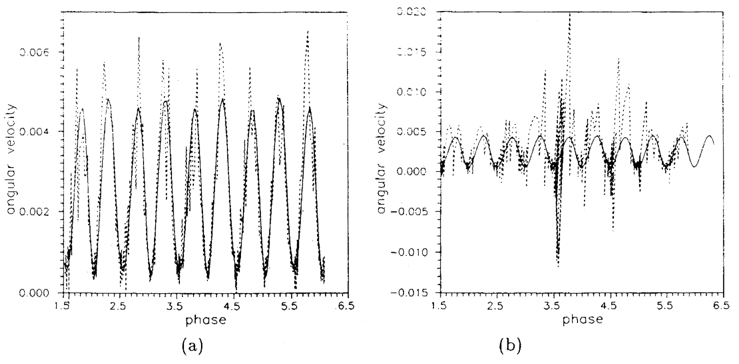

(a) (b)

Fig. 4. The angular velocity as a function of phase. Notation as in Fig. 3. (a)—$\Omega = 10800$, $k_2 = 8$; (b)—$\Omega = 10800$, $k_2 = 6$.

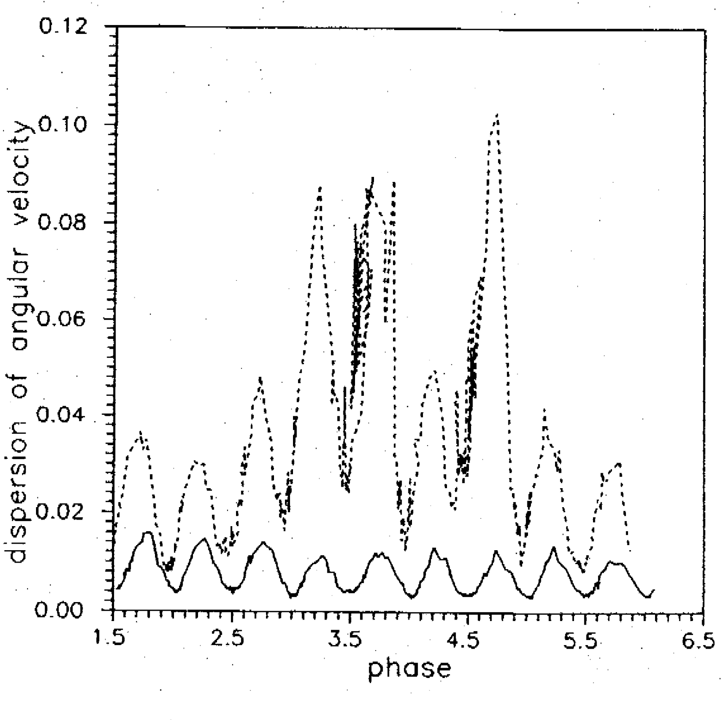

Fig. 5. The dispersion of angular velocity obtained in MD simulations as a function of phase. The solid line — $\Omega = 10800$, $k_2 = 8$; the dashed line — $\Omega = 10800$, $k_2 = 6$.

of increasing angular velocity. The dispersion of ω as a function of phase obtained in MD simulations is shown in Fig. 5 and, like $\omega(\phi)$, it has two maxima per a single period. Therefore, by introducing the phase and the angular velocity, we are able to point the part of the limit cycle for which the influence of internal fluctuations is the most important.

The influence of internal fluctuations on an oscillating system can be also measured if one considers the radius corresponding to MD results scaled by the phenomenological radius for the same phase. For $k_2 = 8$, due to nonequilibrium effects, the average scaled MD radius as a function of phase is nearly constant and equals to 0.88. For $k_2 = 6$ the dispersion of MD radii, which correspond to the same phase is so large that the average value does not give any important information. The distribution functions of the scaled radii of all states obtained in MD simulations are shown in Fig. 6. The distribution obtained for $k_2 = 8$ (the solid line) is compared with the one corresponding to $k_2 = 6$ (the dashed line). In the second case the distribution of radii is very wide. The MD results indicate that two types of fluctuations appear in our system: the short time scale fluctuations related to system's size and the fluctuations associated with the random motion of trajectory in the phase space, which are more pronounced if the limit cycle is less attractive. The fluctuations of the second kind need more time to develop. In order to see more clearly the difference between these types of fluctuations we compared the average dispersion of radius for time intervals

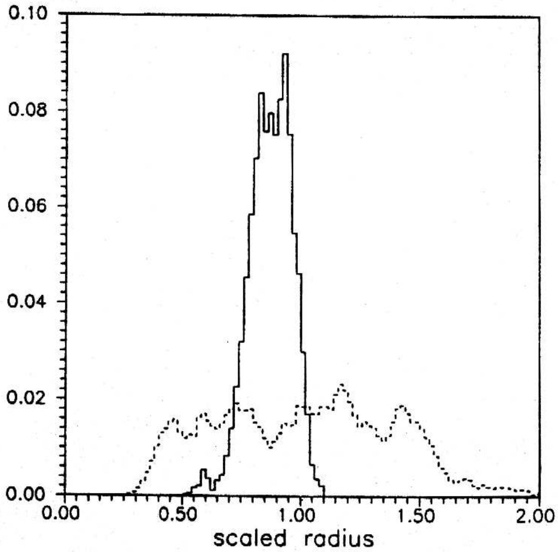

Fig. 6. The comparison of distribution functions of radius obtained in MD simulations for $\Omega = 10800$ and two values of k_2: $k_2 = 8$ (the solid line) and $k_2 = 6$ (the dashed line).

which are t_e long with the dispersion for the whole simulation. For $k_2 = 8$ the average dispersion is about 57% of the total dispersion. For $k_2 = 6$ the average dispersion of radii measured within single interval t_e is only 44% of the total one. It indicates that in the oscillating system with strongly attracting limit cycle ($k_2 = 8$) fluctuations are fully developed at much shorter times (as compared with the period of oscillations) than in the case the limit cycle is weakly attracting ($k_2 = 6$).

4. Propagation of a chemical front in $A + B \rightarrow A + A$ system

A propagating chemical wave front, which consumes reactants ahead and leaves products behind, is one of the simplest manifestations of an organized spatio-temporal structure in a nonhomogeneous chemical system. One of the most widely studied example of a chemical wave front is related to quadratic autocatalysis [16,17,18]:

$$A + B \xrightarrow{k} A + A\,. \tag{11}$$

For this reaction both states: composed of pure A molecules and composed of pure B molecules are stationary; the first one is stable and the other is unstable. Therefore, in an inhomogeneous system, one part of which contains pure A and the other pure B reagent, the interface between A and B propagates into the region composed of pure B. It follows from the reaction scheme (11) that the total number of molecules of A and B remains constant. Let us denote by A and B the concentrations of corresponding species and let N_0 is the total concentration of them ($A+B = N_0$). Having in mind that at each point of space $\boldsymbol{x}$ and at every moment of time t $A(\boldsymbol{x},t)+B(\boldsymbol{x},t) = N_0$, the state of the system is defined by a single concentration only, for example $A(\boldsymbol{x},t)$. The time evolution of an inhomogeneous system with reaction (11) is described by reaction-diffusion equation:

$$\frac{\partial A}{\partial t} = kAB + D\nabla^2 A = kA(N_0 - A) + D\nabla^2 A\,, \tag{12}$$

where k and D denote the rate constant and the diffusion constant, respectively. Introducing the scaled variables: concentration $\alpha = A/N_0$, rate constant $\kappa = N_0 k$, time $\tau = \kappa t$ and the space variable $\boldsymbol{\zeta} = \sqrt{\kappa/D}\boldsymbol{r}$ one can transform Eq. (12) to the form:

$$\frac{\partial \alpha}{\partial \tau} = \alpha(1-\alpha) + \nabla^2 \alpha\,. \tag{13}$$

For the moment let us focus our attention on one dimensional systems only. Let us assume that a stationary wave front propagates along the

x-axis with a constant velocity ν. Its profile may be described in the reference frame moving together with it:

$$\alpha(\boldsymbol{\zeta}, \tau) = \alpha(\zeta_x, \tau) = \alpha(\zeta)\,, \tag{14}$$

where $\zeta = \zeta_x - \nu\tau$. The stationary front profile α as a function of ζ variable satisfies equation:

$$\nu\frac{\partial\alpha}{\partial\zeta} + \frac{\partial^2\alpha}{\partial\zeta^2} + \alpha(1-\alpha) = 0\,. \tag{15}$$

It is known [18] that Eq. (15) admits solutions which are greater or equal than the critical one $\nu_{\min} = 2$. In non-scaled variables transforms to:

$$v_{\min} = 2\sqrt{\kappa D}\,. \tag{16}$$

The particular solution of Eq. (15) which corresponds to $v_{\min}$ is very important because it was shown by Mc Kean [19] that a step-function initial distribution of A evolves into a wave front propagating with this minimal velocity. This result was later generalized by Bramson [20] and by Merkin and Needham [21], who proved that velocity of any front originating from an initial condition, such that the concentration of A vanishes for all ζ greater than some ζ_0, converges to the front with minimal stable velocity. Unfortunately the analytical solution for the profile corresponding to $\nu_{\min}$ is not known [22]. In general it can be shown [23] that if the propagation of front is described by the reaction-diffusion in the form:

$$\frac{\partial\alpha}{\partial t} = \chi_{\varepsilon,s_F}(\alpha)\alpha(1-\alpha) + D\nabla^2\alpha\,, \tag{17}$$

where $\chi_{\varepsilon,s_F}(\alpha)$ is a positive function of α, then the minimum stable velocity for it is given by:

$$v = 2\sqrt{Dn_0\lim_{\alpha\to 0}\chi_{\varepsilon,s_F}(\alpha)}\,. \tag{18}$$

In the following we are concerned with fronts generated by thermally activated reaction (11). It is known that any thermally activated chemical process creates nonequilibrium energy distributions for molecules of both reactant and product [24,25]. The reaction cross section for a thermally activated reaction depends on the energy of reactants and acts like a Maxwell demon, which allows for reactions between the most energetic molecules. In particular, if such reaction proceeds in an adiabatic system and the average temperature of the system as a whole remains constant, than the rate constant becomes different from the value which characterizes the mixture of A and B molecules in which the energy distributions of both reagents are the equilibrium ones [26]. Therefore (*cf.* Eq. (16)) the front velocity may be different than the one calculated using the equilibrium rate constant. In this chapter we consider reactions characterized by different activation energies and steric factors which are selected such that the equilibrium rate constants are the same. If the nonequilibrium effects are negligible than the velocities of fronts associated with such reactions should be equal. We show that if the nonequilibrium effects are taken into account both velocity and width of a front depend on the activation energy. It is worthwhile to add that propagating fronts created by exothermic, thermally activated reactions have been extensively studied as means to produce new materials in so called "High Temperature Synthesis" [27].

First let us consider the influence of nonequilibrium effects on the rate constant of a thermoneutral (the reaction heat is equal to zero), thermally activated reaction $A+B \to 2A$ which proceeds in a homogeneous system. In simulations performed using molecular dynamics for reactive hard spheres a thermally activated process can be described by the line-of-center model [28] according to which a collision between spheres representing A and B may be reactive if the energy of the relative motion of spheres along the line of their centers, calculated in the center of mass reference frame, exceeds the assumed activation energy E_A. It can be shown that the reaction cross section which corresponds to the line-of-center model is defined as:

$$\sigma^*_{A,B} = \begin{cases} \frac{1}{4} s_F d^2 \left(1 - \frac{E_A}{E_C}\right) & \text{for } E_C \geq E_A \\ 0 & \text{for } E_C < E_A \end{cases}, \tag{19}$$

where s_F is the steric factor, d and m denote the diameter and mass of a sphere and

$$E_C = \frac{1}{4}(\vec{v}_A - \vec{v}_B)^2 m \,,$$

where $\vec{v}_A$ and $\vec{v}_B$ are velocities of colliding spheres. If the velocity distributions of A and B are represented by Maxwellians at temperature T_0 than the rate constant $k(T_0)$ reads:

$$k(T_0) = 4d^2 s_F g_{AB} \left(\frac{\pi k_B T_0}{m}\right)^{\frac{1}{2}} \exp\left(-\frac{E_A}{k_B T_0}\right), \tag{20}$$

where g_{AB} is the value of the radial distribution function for the distance d.

The theoretical description of nonequilibrium effects in an adiabatic system with a thermally activated reaction can be significantly simplified if one assumes that the energy distribution for molecules representing reactant B can be approximated by a Maxwellian ($f_{M,T_B(t)}$), which corresponds to a time dependent temperature $T_B(t)$ [25,29]. The considered system is composed of A and B molecules only so we have the following relationship between energy distributions of molecules of reactant and product:

$$N_0 f_{M,T_0}(v) = A f_A(v) + B f_{M,T_B}(v)\,. \tag{21}$$

Now the kinetic equation for A reads:

$$\begin{aligned}\frac{dA}{dt} &= k(A(t))AB = AB\int \sigma^* f_A(v_1) f_{M,T_B(t)}(v_2)dv_1dv_2d\Omega \\ &= B\int \sigma^*(N_0 f_{M,T_0(t)}(v_1) - B f_{M,T_0(t)}(v_1)) f_{M,T_B(t)}(v_2)dv_1dv_2d\Omega \\ &= N_0 B s_F 4d^2 g\left(\frac{\pi k_B(T_0+T_B(t))}{2m}\right)^{1/2}\exp\left(-\frac{2E_A}{k_B(T_0+T_B(t))}\right) \\ &\quad -B^2 s_F 4d^2 g\left(\frac{\pi k_B T_B(t)}{m}\right)^{1/2}\exp\left(-\frac{2E_A}{k_B T_B(t)}\right)\,. \end{aligned}\tag{22}$$

This equation has to be completed by the equation describing the dynamics of T_B. Such equation comes from the balance for the energy density of B in which the energy losses in reactive collisions (a reacting molecule of B is transformed into product A) and the energy exchange between A and B molecules in nonreactive collisions are considered. The corresponding formulae are derived in [29]. In the scaled variables defined as:

$$\varepsilon = \frac{E_A}{k_B T_0},\quad \beta = \frac{B}{N_0} = 1-\alpha, \xi = \frac{T_B}{T_0} \quad \text{and} \quad \tau = 4d^2 g_{AB}\left(\frac{\pi k_B T_0}{m}\right)^{\frac{1}{2}} N_0 t$$

one obtains the following set of kinetic equations:

$$\frac{d}{d\tau}\beta = -\beta s_F\left(\frac{1}{2}(1+\xi)\right)^{\frac{1}{2}}\exp\left(-\frac{2\varepsilon}{1+\xi}\right) + \beta^2 s_F \xi^{\frac{1}{2}}\exp\left(-\frac{\varepsilon}{\xi}\right)\,, \tag{23}$$

$$\begin{aligned}\frac{d}{d\tau}\xi &= \frac{2}{3}\Bigg\{-s_F\left(\frac{1+\xi}{2}\right)^{\frac{1}{2}}\exp\left(-\varepsilon\frac{2}{1+\xi}\right)\xi\left(\frac{\xi}{2(1+\xi)} + \varepsilon\frac{2\xi}{(1+\xi)^2}\right) \\ &\quad + s_F\beta\xi^{\frac{1}{2}}\exp\left(-\frac{\varepsilon}{\xi}\right)\xi\left(\frac{1}{4}+\frac{\varepsilon}{2\xi}\right) + \left(\frac{1+\xi}{2}\right)^{\frac{1}{2}}(1-\xi) \\ &\quad - s_F\left(\frac{1+\xi}{2}\right)^{\frac{1}{2}}(1-\xi)\left(1+\varepsilon\frac{2}{1+\xi}\right)\exp\left(-\varepsilon\frac{2}{1+\xi}\right)\Bigg\}\,. \end{aligned}\tag{24}$$

It can be easily solved numerically for any values of ε and s_F. Having $\beta(\tau)$ and $\xi(\tau)$ one can calculate the energy of A molecules

$$e_A(\tau) = \frac{1-\beta(\tau)\xi(\tau)}{1-\beta(\tau)} \tag{25}$$

and the scaled nonequilibrium rate constant:

$$\chi = \frac{k}{k(T_0)} = \frac{\exp(\varepsilon)}{1-\beta(\tau)}\left[\left(\frac{1}{2}(1+\xi(\tau))\right)^{\frac{1}{2}} \times \exp\left(-\frac{2\varepsilon}{1+\xi(\tau)}\right) - \beta(\tau)\Big(\xi(\tau)\Big)^{\frac{1}{2}} \exp\left(-\frac{\varepsilon}{\xi(\tau)}\right)\right]. \tag{26}$$

The functions $e_A(\alpha)$, $\xi(\alpha)$ and $\chi(\alpha)$ are shown by the dashed line in Fig. 7. In order to check how accurate is this simple phenomenology we performed molecular dynamics simulations creating many individual reaction paths. On the basis of these results we obtained the average concentrations of A and B as functions of time $(\langle A\rangle(t), \langle B\rangle(t))$ and the average kinetic energies per a molecule of reagent $(\langle e_A(t)\rangle, \langle e_B(t)\rangle)$. The numerical technique is the same as applied in [30] to study the nonequilibrium effects associated with reaction $A + A \to$ *products*. If the average concentrations are known it is easy to calculate the nonequilibrium rate constant as a function of time (or as a function of concentration of A, which increases monotonically with time):

$$k(\langle A\rangle(t)) = \frac{1}{\langle A\rangle(t)\langle B\rangle(t)}\frac{d\langle A\rangle}{dt}\,. \tag{27}$$

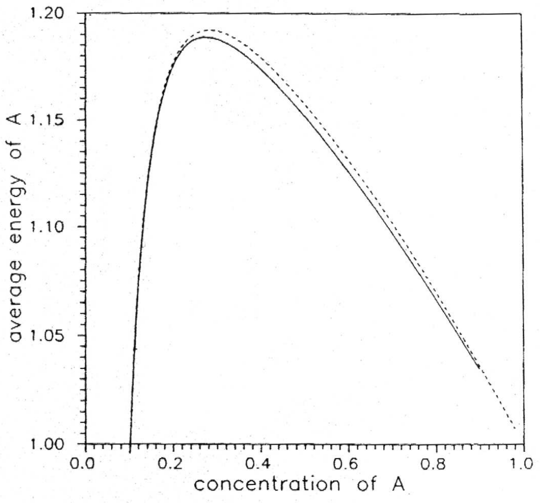

Fig. 7. The average energy of A particles, scaled by $\frac{3}{2}k_BT_0$, for a homogeneous system with reaction (11) characterized by $\varepsilon = 1$ and $s_F = 1$ shown as a function of α. Initially $\alpha(\tau = 0) = 0.1$ and $\xi(\tau = 0) = 1$. The solid line — molecular dynamics simulations, the dashed line — solution of phenomenological equations (Eqs. (23),(24)).

The simulations has been performed for a system of $N_0 = 1000$ hard spheres with the diameter 5 and mass 32 a.u. placed in a cube with the side length $17.5{*}d$ what corresponds to the packing fraction $\eta = 0.098$. At the beginning of each reaction path 900 spheres represented B and the remaining 100 — A.

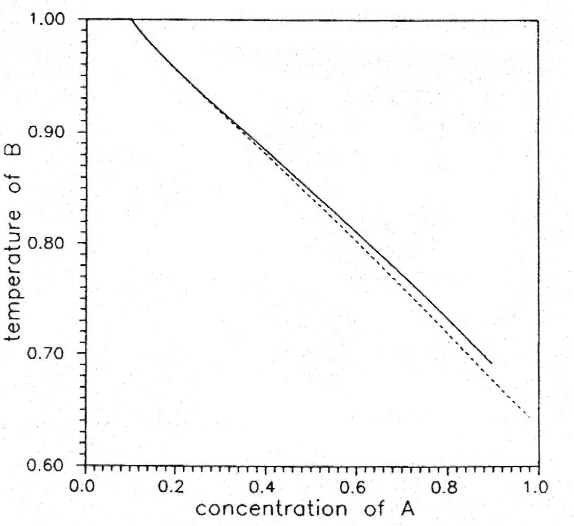

Fig. 8. The temperature of B particles scaled by T_0 for a homogeneous system with reaction (11) characterized by $\varepsilon = 1$ and $s_F = 1$ shown as a function of α. Initially $\alpha(\tau = 0) = 0.1$ and $\xi(\tau = 0) = 1$. Notation as in Fig. 7.

The rate constant calculated on the basis of Eq. (27) and scaled to the equilibrium value (20) is shown in Fig. 9 (here $E_A = 2k_BT_0$). Contrary to the reaction $A + A \rightarrow$ *products* for which the nonequilibrium effects always decrease the rate constant [24,26], for reaction (11) we observe that the rate constant as a function of concentration of A rapidly increases from its equilibrium value at the initial stage of reaction. It has a maximum and than its decay is linear. Close to the point in which concentrations of A and B are the same the rate constant is equal to its equilibrium value again and as reaction progress the nonequilibrium contribution to it becomes negative. The effect can be explained as follows: the rate constant depends on the velocity distributions for both A and B. If the concentration of A is small than the increase in $\langle e_A \rangle$ plays more important role than a small decrease in $\langle e_B \rangle$ (compare Figs. 7 and 8) and the rate constant is larger than the equilibrium one. On the other hand if concentration of A is large than $\langle e_A \rangle$ is close to the equilibrium value, but the energy of B molecules is significantly decreased (Fig. 8). As the result the rate constant is smaller than the equilibrium one.

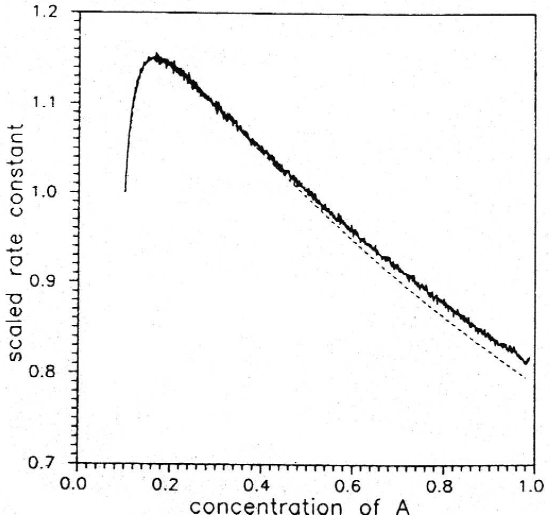

Fig. 9. The rate constant scaled by its equilibrium value for a homogeneous system with reaction (11) characterized by $\varepsilon = 2$ and $s_F = 1$ shown as a function of α. Initially $\alpha(\tau = 0) = 0.1$ and $\xi(\tau = 0) = 1$. Notation as in Fig. 7.

We have found that the agreement between results of simulation and the theory based on the existence of the nonequilibrium temperature of B is very good. Therefore, in the following we shall use Eqs. (23),(24) to study the influence of nonequilibrium effects on the rate constant. Fig. 10 shows the scaled rate constant χ (*cf.* Eq. (26)) as a function of concentration of A for a system characterized by $E_A = 2k_BT$. Three different initial conditions has been considered $\alpha(\tau = 0) = 0.02$, $\alpha(\tau = 0) = 0.1$ and $\alpha(\tau = 0) = 0.2$. It can be noticed that, irrespectively of the initial conditions, the scaled rate constant χ as a function of concentration of A converges to the universal curve $\chi_{s_F,\varepsilon}(\alpha)$ after a short initial period. If a numerical solution of Eqs. (23),(24) is known than $\chi_{s_F,\varepsilon}$ may be approximated by a polynomial fit and a particular form of it is given in Table I for the system studied.

Reaction (11) is thermoneutral so all collisions (including reactive ones) are elastic and therefore the periodic expansion can be used to enlarge the size of simulated system. The results presented below were obtained by a periodic expansion of the same trajectory, which was used to simulate the nonequilibrium effects in a homogeneous system. Simulations were performed for a system expanded by 12 side lengths in x- and in y-directions and by 100 side lengths in the z-direction. Therefore the total number of spheres considered was $14,400,000$. A few simulations were done for a smaller system in order to check if the scale of expansion affects the results. A good agreement between different simulations has been obtained.

TABLE I

The parameters describing nonequilibrium effects in a homogeneous system with reaction $A + B \to 2A$. The values of ε and s_F are the same as used to study the propagation of a chemical wave front ($s_F = 0.03\exp(\varepsilon)$).

ε	$\lim_{\tau\to\infty}\xi$	$\chi_{s_F,\varepsilon}(\alpha)$(numerical fit)
0.0	0.9924	$1.0018 - 0.0036\alpha - 0.0002\alpha^2$
1.0	0.9771	$1.0017 - 0.0337\alpha - 0.0006\alpha^2$
2.0	0.9623	$1.0495 - 0.1020\alpha + 0.0054\alpha^2$
2.5	0.9553	$1.0734 - 0.1550\alpha + 0.0154\alpha^2$
3.0	0.9486	$1.1032 - 0.2250\alpha + 0.0338\alpha^2$
3.5	0.9423	$1.1399 - 0.3160\alpha + 0.0640\alpha^2$

For an expanded system the periodic boundary conditions were used in x- and y-directions. Modified periodic boundary conditions were used in the z-direction: the chemical identity parameter of a sphere crossing the boundary of an expanded system was reversed. In order to observe front propagation the initial concentration of reactants were nonhomogeneous in the z-direction. Part of the simulations started form an initial concentrations described by a step-function: all the spheres, for which $z \leq z_0$ were marked as A, all the other as B. In other simulations there was a wide interval of z within which the initial concentrations of both reactants were different from zero. To analyze the results, the system was divided into 500 slices perpendicular to the z- axis. The fraction of particles of each reactant is averaged over each slice.

The same numerical technique was used in our previous papers to simulate propagation of a chemical wave front in a system with reaction (11) [31,32]. In these papers we found that if the probability of reactive collision is large than a chemical front propagates faster than it is predicted by a parabolic reaction-diffusion equation Eq. (16). The effect seems to be related with nonequilibrium character of diffusion process. Here we are concerned with much slower reactions, for which we can expect that the parabolic reaction-diffusion equation correctly describes system's evolution. In our simulations we considered the reactions for which $s_F = 0.03\exp(\varepsilon)$.

Fig. 11 shows a few snapshots of well developed front of concentration of A obtained in simulations. The calculations were performed for $\varepsilon = 0.0$ and $s_F = 0.03$ (Fig. 11(a)) and for $\varepsilon = 3.0$ and $s_F = 0.03\exp(3)$ (Fig. 11(b)). It can be seen that the activated front propagates faster than the nonactivated one. In order to measure front's velocity and width we use the following method. The values of α and β can be precisely defined for each slice at any

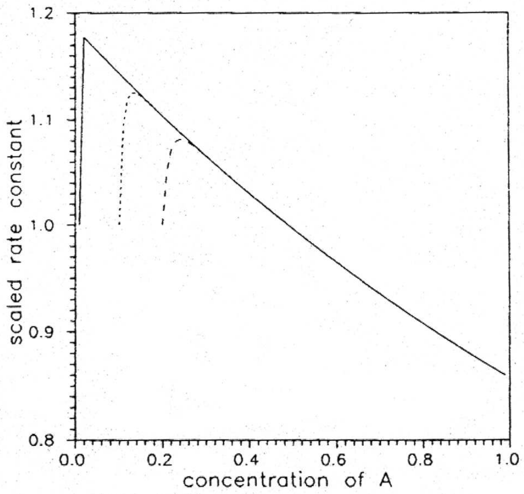

Fig. 10. The rate constant scaled by its equilibrium value for a homogeneous system with reaction (11) characterized by $\varepsilon = 3$ and $s_F = 1$ shown as a function of α. The lines show the solution of Eqs. (23),(24) for $\xi(\tau = 0) = 1$ and the following values of $\alpha(\tau = 0)$: $\alpha(\tau = 0) = 0.01$ — the solid line, $\alpha(\tau = 0) = 0.1$ — the short dashed line, $\alpha(\tau = 0) = 0.2$ — the long dashed line.

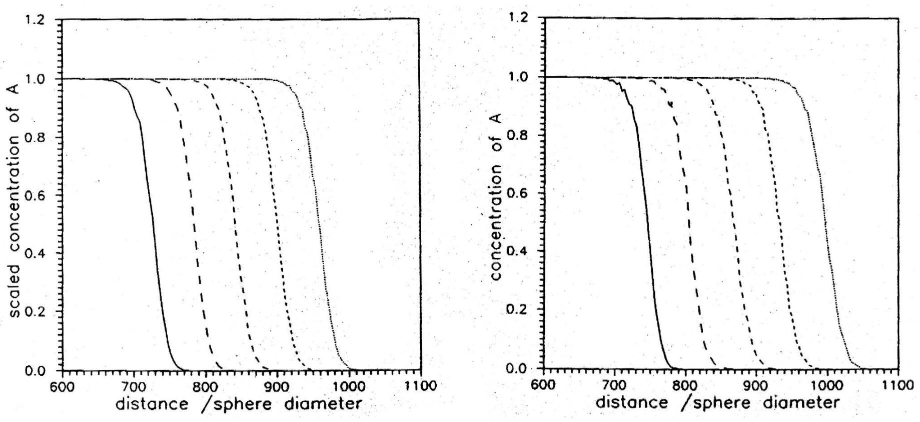

(a) (b)

Fig. 11. The propagation of a chemical wave front in a system characterized by $\eta = 0.098$. The parameters of reaction are: $\varepsilon = 0.0$ and $s_F = 0.03$ (Fig. 11(a)) and $\varepsilon = 3.0$ and $s_F = 0.03 \exp(3)$ (Fig. 11(b)). The initial distribution of A and B particles is the same in both cases. The curves from the left one to the right one correspond to times: 1211 ps, 1419 ps, 1629 ps, 1837 ps, and 2046 ps, respectively.

time t. We can define a new quantity $\gamma(z)$ as:

$$\gamma(z_i,t) = \begin{cases} \alpha(i,t) & \text{if} \quad \alpha(i,t) \leq 0.5 \\ \beta(i,t) & \text{if} \quad \alpha(i,t) > 0.5 \end{cases} , \tag{28}$$

where z_i is the mean value of z corresponding to the i-th slice. $\gamma(z,t)$ is a localized function of z. We can define the front position $\langle z\rangle(t)$ and width $\langle(\delta z)^2\rangle(t)$ as:

$$\langle z\rangle(t) = \frac{\sum\limits_i z_i\gamma(z_i,t)}{\sum\limits_i \gamma(z_i,t)} \tag{29}$$

and

$$\langle(\delta z)^2\rangle(t) = \frac{\sum\limits_i z_i^2\gamma(z_i,t)}{\sum\limits_i \gamma(z_i,t)} - \langle z\rangle^2(t) \tag{30}$$

The front's position and width as functions of time are presented in Figs. 12 and 13, respectively. It can be noticed that front's width rapidly increases after initialization of the front and then decreases to a constant value what indicates that the front has approached its stationary profile. In our simulations the reaction parameters (ε, s_F) have been selected that

$$s_F \exp(-\varepsilon) = \text{const.} \tag{31}$$

which means that if the nonequilibrium effects are neglected the minimum stable velocity (Eq. (16)) for all fronts considered should be the same. Also the front's width commonly defined as:

$$\delta \cong \sqrt{\frac{D}{k}} \tag{32}$$

should be equal each other. The results presented in Figs. 12 and 13 clearly indicate that for fronts generated by thermally activated reactions which satisfy condition (31) both velocity and width are increasing functions of activation energy. The data obtained in our simulations are given in Tables II and III. One can see that front's width changes with increasing activation energy more rapidly than the rate constant.

In order to describe quantitatively the influence of nonequilibrium effects on the propagation of a chemical wave front generated by a thermally activated reaction one may assume that the nonequilibrium rate constant as a function of α is the same as in a homogeneous system and it is given by $\chi_{s_F,\varepsilon}(\alpha)$. To test if this assumption is justified we measured the energy of

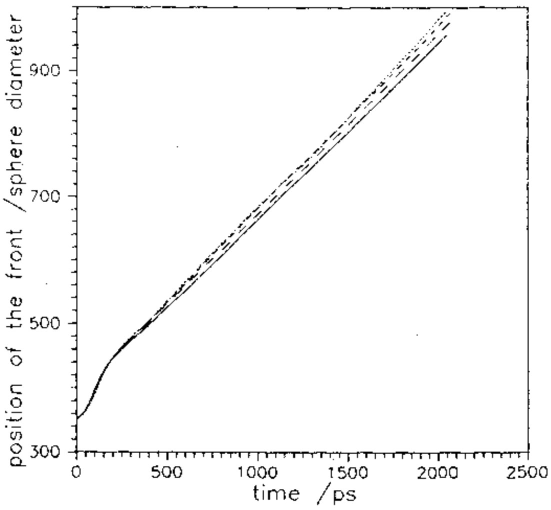

Fig. 12. The position of the front as a function of time for the system of $N = 14,400,000$ particles characterized by $\eta = 0.098$ and $s_F = 0.03\exp(\varepsilon)$; solid line — $\varepsilon = 0$, the long dashed line — $\varepsilon = 1$, the short dashed line — $\varepsilon = 2$, the dotted line — $\varepsilon = 3$.

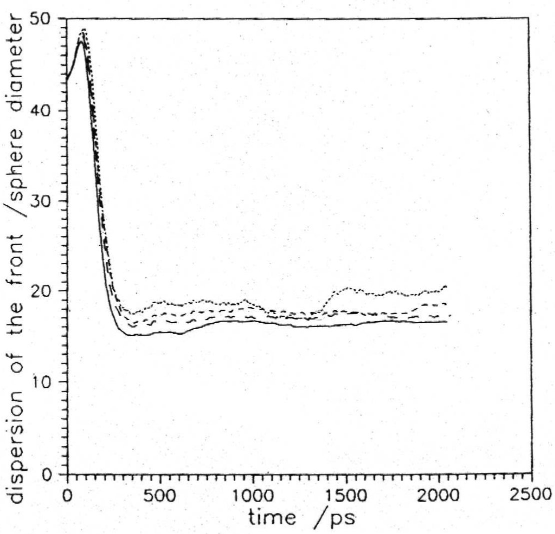

Fig. 13. The dispersion of the front as a function of time for the system of $N = 14,400,000$ particles characterized by $\eta = 0.098$ and $s_F = 0.03\exp(\varepsilon)$; solid line — $\varepsilon = 0$, the long dashed line — $\varepsilon = 1$, the short dashed line — $\varepsilon = 2$, the dotted line — $\varepsilon = 3$.

A particles in every slice along the z-axis. The measurements were repeated for 25 snapshots of the front. The average energy of A particles as a function of α is marked by points in Fig. 14. We compare the results obtained for $\varepsilon = 0.0$ (small symbols) with those for $\varepsilon = 3.0$ (large symbols). The lines show $e_A(\alpha)$ calculated on the basis of the "universal" function $\xi(\alpha)$ obtained from Eqs. (23),(24) for a homogeneous system. As expected, the average energy of A in the front is a decreasing function of α. The molecules of A appear in a highly energetic reactive collisions with B particles and their energy (in average) is higher than $\frac{3}{2}k_BT_0$. As front moves and the reaction develops more energy is transferred from A to B particles and e_A approaches the equilibrium value. The agreement between $\langle e_A\rangle$ obtained for front profile and the phenomenology is very good except for the point corresponding to the lowest concentration $(0.0 < \alpha < 0.1)$. Moreover the dispersion of $\langle e_A\rangle$ at this point is by an order of magnitude higher than for the others.

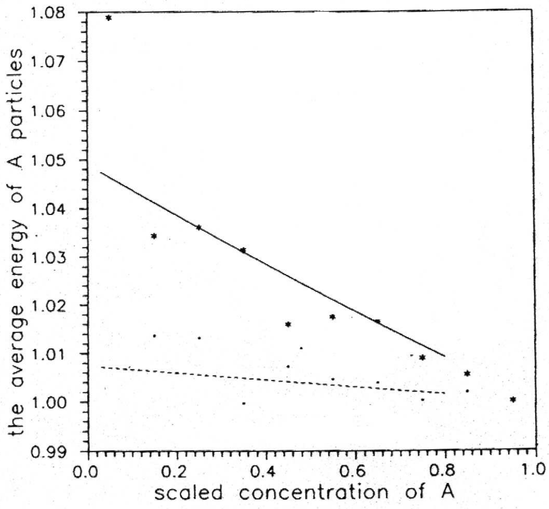

Fig. 14. The points mark the average energy of A particles in the chemical front, scaled by $\frac{3}{2}k_BT_0$, as a function of α for the system of $N = 14,400,000$ particles characterized by $\eta = 0.098$ and $s_F = 0.03\exp(\varepsilon)$; the small dots — $\varepsilon = 0$, the big dots — $\varepsilon = 2.5$. The lines show $e_A(\alpha)$ obtained from equation describing a homogeneous system (Eqs. (23),(24)).

The numerical fit for $\chi_{\varepsilon,s_F}(\alpha)$ indicates that, due to the nonequilibrium effects, for the set of reactions satisfying (31), the front's velocity is an increasing function of activation energy. The results are given in Table II. First let us notice that, due to the fact that the considered reactions are still fast if compared to diffusion, the velocities of fronts obtained for $\varepsilon = 0.0$ are slightly larger than the minimal stable velocity calculated from Eq. (16). The dispersion of the front shown in Fig. 13 indicates that the simulated front has reached its stationary form, so the difference in velocities does not come from transient effect. In order to see the influence of nonequilibrium effects on the velocity it is convenient to introduce the velocity scaled to its value for $\varepsilon = 0.0$ separately for simulations and phenomenology. The numbers shown in Table II say that the phenomenological description introduced by us slightly underestimates front's velocity, but nevertheless may be applied as a first approximation of the nonequilibrium effects. It is estimated that the error of scaled velocities obtained in simulations is around 0.02, thus the agreement is rather good.

TABLE II

The velocity (measured in $\frac{d}{ps}$ of a front generated by a thermally activated reaction $A + B \rightarrow A + A$. Comparison between molecular dynamics simulation and theory ($s_F = 0.03\exp(\varepsilon)$).

ε	v_{MD}	v(Eq. (18))	$\frac{v_{\mathrm{MD}}}{v_{\mathrm{MD},\varepsilon=0}}$	$\frac{v}{v_{\varepsilon=0}}$ (Eq. (18))
0.0	0.280	0.247	1.00	1.000
2.0	0.284	0.235	1.01	1.024
2.5	0.293	0.255	1.05	1.035
3.0	0.307	0.263	1.10	1.067

TABLE III

The dispersion (measured in d) of a front generated by a thermally activated reaction $A + B \rightarrow A + A$. Comparison between molecular dynamics simulation and theory ($s_F = 0.03\exp(\varepsilon)$).

ε	δ_{MD}	δ_{num}	$\frac{\delta_{\mathrm{MD}}}{\delta_{\mathrm{MD},\varepsilon=0}}$	$\frac{\delta_{\mathrm{num}}}{\delta_{\mathrm{num},\varepsilon=0}}$
0.0	16.6 ± 0.08	13.80	1.00	1.00
2.0	17.2 ± 0.12	14.30	1.04	1.04
3.0	19.7 ± 0.20	14.90	1.19	1.08

The dispersions of fronts obtained for different ε are shown in Table III. The phenomenological values of it were calculated from the numerical solution of Eq. (18) with the appropriate χ_{ε,s_F} from Table I. The dispersion is also an increasing function of ε and the rate it increases is about twice as large as for the velocity. This results can be easily understood. The front's velocity depends on the nonequilibrium effects by the $\lim_{\alpha\to 0}\chi_{\varepsilon,s_F(\alpha)}$ only, whereas the values of rate constant for both $\alpha \rightarrow 0$ and $\alpha \rightarrow 1$ have influence on front's width. Let us notice that combining Eq. (16) with Eq. (32) one obtains that $v_{\rm min} * \delta$ does not depend on the rate constant. This conclusion is clearly not hold for fronts generated by thermally activated reactions.

5. Conclusions

In this paper we have studied examples of chemical systems for which the phenomenological description is not sufficient and microscopic simulations give additional information on system's evolution. In the first part we were concerned with molecular dynamics simulations of a model of oscillatory system. The MD simulation allowed us to study the influence of fluctuations on simple periodic oscillations. Instead of a closed line corresponding to the limit cycle, MD results are dispersed as a "ring"-like structure forming the phase portrait of the system influenced by internal fluctuations. We introduced an approximate quantitative description of fluctuations based on phase dependent radius and phase. As expected we have found that the strength of fluctuations decreases with the system's size. By considering two cases in which (according to the phenomenology) the limit cycle is weakly and strongly attractive we have been able to distinguish two types of fluctuations. One of them is related to the volume of the system whereas the other characterizes the random motion of the MD trajectory in the phase space and depends on phenomenological parameters (k_2 in our case). These two types of fluctuations differ by time scales. The size dependent fluctuations appear on much shorter time scale than the other. We have introduced the phase and studied the influence of fluctuations on the angular velocity. It has been shown that the regions in which angular velocity increases are more affected by the internal fluctuations than the other part of the cycle.

In the second part of this paper we have been concerned with the influence of nonequilibrium effects on the propagation of the wave front. We have considered a set of thermoneutral thermally activated reactions for which the activation energies are different but the equilibrium rate constants remain the same. Therefore, if nonequilibrium effects are neglected, then the chemical wave fronts generated by these reactions should propagate with equal velocities. The results of molecular dynamics simulations indicate that both front's velocity as well as its width are increasing functions of the activation energy. It is also observed that the influence of nonequilibrium effects on front width is more important that on front's velocity.

In order to understand these results we have performed simulations of the influence of nonequilibrium effects on the rate constant of reaction $A+B \rightarrow A+A$ proceeding in a homogeneous system. We have found that for low concentration of product A the rate constant is larger than the equilibrium value what can be explained by the presence of nonequilibrium effects, but if

$B < A$ these effects decrease it. As shown in [23], the front's velocity depends on the rate constant for small concentration of A, thus it should increase due to the nonequilibrium effects. The front's width is larger than for a system in which the nonequilibrium effects are absent, because it takes longer for reaction to terminate. These results are in qualitative agreement with simulations, but it seems that phenomenology underestimates the observed effects. We believe that an additional contribution to front's velocity may come from the nonequilibrium diffusion constant of reactant A. In this paper we have assumed that this diffusion constant does not change along the front. The present studies on nonequilibrium diffusion [33] indicate that, for equal masses of reactants and activation energies in the range considered here the influence of nonequilibrium effects on diffusion is less important than on the rate constant. Underestimation of front's velocity by phenomenology may be also related to the randomness in energy of A particles for the initial part of the front. The dispersion in e_A is very high and it may give a positive contribution to front's velocity.

REFERENCES

[1] *Spatial Inhomogeneities and Transient Behaviour in Chemical Systems*, Eds. P. Gray, G. Nicolis, F. Baras, P. Borckmans and S.K. Scott, Manchester University Press, 1990.

[2] G. Nicolis, I. Prigogine, *Self-Organization in Non-equilibrium Systems*, Wiley, New York 1977.

[3] Nonequilibrium Chemical Dynamics, from Experiment to Microscopic Simulations, Eds. F. Baras and D. Walgraef, published as *Physica A* **188**, (1992).

[4] *Far-form-Equilibrium Dynamics of Chemical Systems*, Eds. J. Popielawski and J. Gorecki, World Scientific, Singapore 1991.

[5] *Far-form-Equilibrium Dynamics of Chemical Systems*, Eds.: J. Gorecki, A.S. Cukrowski, A.L. Kawczynski and B. Nowakowski, World Scientific, Singapore 1994.

[6] *Dynamism and Regulation in Nonlinear Chemical Systems*, Eds. M.A. Marek, S.C. Muller, T. Yamaguchi and K. Yoshikawa, North Holland 1995.

[7] *Chemical Waves and Patterns*, Eds. R. Kapral and K. Showalter, Kluwer Academic Publishers, Dordrecht 1995.

[8] R. Kapral, *J. Math. Chem.* **6**, 113 (1991); R. Kapral, A. Lawnczak, P. Masiar, *Phys. Rev. Lett.* **66**, 2539 (1991).

[9] G.A. Bird, *Molecular Gas Dynamics*, Clarendon, Oxford 1976.

[10] J. Gorecki, J. Gryko, *Comput. Phys. Commun.*, **54**, 245 (1989).

[11] M.P. Allen, D.J. Tidesley, *Computer Simulations of Liquids*, Clarendon Press, Oxford 1987.

[12] J. Gorecki, *Mol. Phys. Rep.*, **10**, 48 (1995).

[13] J. Gorecki, A.L. Kawczyński, *Polish J. Chem.* **71**, 1553 (1997).

[14] J. Boissonade, *Physica A* **113**, 607 (1982).

[15] Y. Kuramoto, *Prog. Theor. Phys.* **52**, 711 (1974); G. Nicolis, M. Malek Mansour, *Phys. Rev.* **29A**, 2845 (1984); K. Kitahara, K. Seki, S. Suzuki, *J. Phys. Soc. Japan*, **59**, 2309 (1990); J. Gorecki, K. Kitahara, *Physica A* **245**, 164 (1997).

[16] R.A. Fisher, *Ann. Eugenics* **7**, 335 (1937); A. Kolmogorov, I. Petrovsky, N. Piskunov, *Bull. Univ. Moscow Ser. Int.* **Sec. A1**, 1 (1937).

[17] P. Gray, K. Showalter, S.K. Scott, *J. Chim. Phys.* **4**, 1329 (1987).

[18] S.K. Scott, K. Showalter, in *Chemical Waves and Patterns*, eds. R. Kapral, K. Showalter, Kluwer Academic Publishers, Dordrecht 1995.

[19] H.P. McKean, *Commun. Pure Appl. Math.* **28**, 323 (1975).

[20] M.D. Bramson, *Commun. Pure Appl. Math.* **31**, 531 (1978).

[21] J.H. Merkin, D.J. Needham, *J. Eng. Math.* **23**, 343 (1989).

[22] An approximate expression was given in J.D. Murray, *Mathematical Biology*, Springer, Berlin 1989.

[23] R.D. Benguria, M.C. Depassier, *Phys. Rev. Lett.* **77**, 1171 (1996).

[24] I. Prigogine, E. Xhrouet, *Physica* **15**, 913 (1949); for the recent references see papers in *Far-form-Equilibrium Dynamics of Chemical Systems*, Eds. J. Gorecki, A.S. Cukrowski, A.L. Kawczynski and B. Nowakowski, World Scientific, Singapore 1994.

[25] J. Gorecki, B.C. Eu, *J. Chem. Phys.* **97**, 6695 (1992).

[26] J. Gorecki, J. Popielawski, A.S. Cukrowski, *Phys. Rev.* **A 44**, 3791 (1991).

[27] see for example J.A. Pojman, V.M. Ilyashenko, A.M. Khan, *Physica* **D84**, 260 (1995); J.A. Pojman, V.M. Ilyashenko, A.M. Khan, *J. Chem. Soc. Faraday Trans.* **92**, 2825 (1996); G. Bowden, M. Garbey, V.M. Ilyashenko, J. Pojman, S.E. Solovyov, A. Taik, V.A. Volpert, *J. Phys. Chem.* **101**, 678 (1997).

[28] R.D. Present, *J. Chem. Phys.* **31**, 747 (1959).

[29] J. Gorecki, *J. Chem. Phys.* **98**, 7269 (1993).

[30] J. Gorecki, *J. Chem. Phys.* **95**, 2041 (1991).

[31] J. Gorecki, *Physica* **D84**, 171 (1995).

[32] J. Gorecki, J.N. Gorecka, *Acta Phys. Pol.* **B26**, 1177 (1995).

[33] B. Nowakowski, A. Lemarchand, *J. Chem. Phys.* **106**, 3965 (1997).